18

Advances in laser-induced plastic deformation processes

A.J. BIRNBAUM, S. VIKELIC and
Y. LAWRENCE YAO, Columbia University, USA

Abstract: Although myriad laser processes take advantage of the ability to convert photon energy into thermal energy resulting in a local increase in temperature, e.g. laser cutting, drilling, welding, in a sense these processes represent a direct energy conversion from laser energy to task. However, when converting laser energy to desired, controllable mechanical deformation, there exist what may be thought of as intermediate steps that arise in the process. This chapter aims to give a brief background and review recent advances for three processes: laser forming, laser shock-peening and laser peen forming. All three of these processes utilize laser energy in order to induce plastic deformation resulting in either a desired final part geometry, desirable material properties/performance or both.

Key words: laser forming, laser shock peening (LSP), thermal forming, plasticity.

18.1 Introduction

Laser forming (LF) is a process which utilizes transient, non-uniform temperature distributions in order to produce controllable deformation and is a topic of ongoing research. It is seen as having definite potential for low to medium yield production or rapid prototyping due to its inherent flexibility. This flexibility stems from the fact that it is a non-contact process, and as such no external hard tooling is required. Furthermore, since it is a thermally based process, materials that have been traditionally challenging to form by mechanical means, such as titanium- or nickel-based super alloys, which are utilized regularly in the aerospace industry, can be readily formed via LF. Recent advances to be discussed include the effects of material anisotropy, free edges, clamping/support, microstructural evolution, specimen geometry, numerical strategies and process design.

Micro-scale laser shock peening and laser peen forming are non-thermal processes that introduce compressive residual stresses into the target material for the improvement of fatigue life and wear resistance under cyclic loading. Furthermore, laser peen forming induces controllable geometric curvature in addition to the desired material response. In recent times research has focused on the micro-scale response and thus it has been necessary to take

into account material anisotropy as well as heterogeneity as the beam spot size is on the order of the grain size. The advances discussed will indeed focus on the implications of implementing this process at the micro-scale. Topics of discussion include material-based effects such as crystallographic orientation and the presence of grain boundaries as well as processing strategies such as dual sided processing vs. traditional single surface implementation. Furthermore, process induced global and locally induced forming effects and their implications for residual stress distributions and fatigue performance are presented as well. Finally, recent advances in predictive capabilities via the implementation of various numerical strategies are put forth.

18.2 Laser forming

18.2.1 Historical perspective

Laser forming (LF) evolved from more mature, but less sophisticated thermo-mechanical forming processes. Specifically, manual application of an oxyacetylene torch for forming steel plates for the ship building industry has been used for some time and is seen as the precursor to LF. However, the flame bending process is highly uncontrollable and successful implementation relies on an extremely skilled worker requiring literally years of experience. One of the earliest references to the laser forming process in literature is found in Namba (1986) where, using a CO_2 laser, he proposes the active deformation mechanism (later referred to as the temperature gradient mechanism). Additionally, Namba performed a limited parametric study examining the effects of varying the laser scan velocity, sheet thickness and number of laser scans on the bending deformation in AISI 304 stainless steel sheets. Another early, major investigation was undertaken by Masubichi (1992) at MIT for the purposes of forming large thick plates for the ship-building industry. This effort included a systematic study of process parameters and their effects on the final bending deformation.

18.2.2 Physical description of process

Laser forming (LF) is accomplished via the local impingement of a defocused continuous-wave (CW) laser beam on the surface of a ductile (almost exclusively metallic) work piece which is continuously translated at a relative velocity to the beam. Figure 18.1 schematically depicts the following description of the process. Depending on the material system being processed and the laser wavelength being utilized, a portion of the incident energy is reflected, and a portion absorbed. At macroscopic scales, i.e. characteristic dimensions of the work piece are several orders of magnitude greater than the wavelength of the incident beam, and particularly for metals, the light-

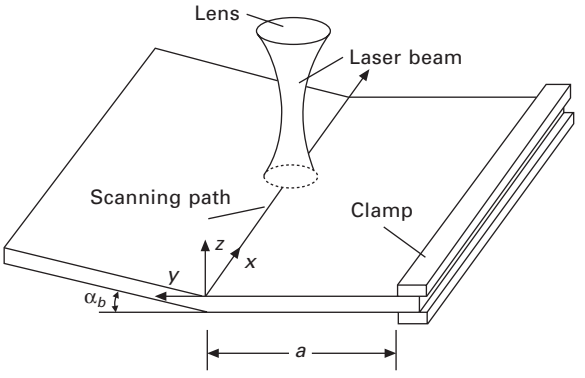

18.1 Schematic of laser-forming process.

matter interaction occurs over tens of nanometers and can be assumed to be occurring exclusively at the part surface.

As the impingement of the beam is limited to within the spot diameter of the laser, the portion of the material within or in close proximity to the location(s) of incidence experience stresses that may exceed the material's flow stress and thus result in the local generation of compressive plastic strains at highly elevated temperatures and is accompanied by global counter-bending (convex toward the laser). It should be noted, that the process parameters; the laser power, scan velocity and spot size are designed such that the resulting maximum temperature for the processed material-geometry combination does not exceed the melting temperature. Therefore, no local melting occurs, and the problem is restricted to one of thermo-elasticity/inelasticity.

Depending on the geometry, as well as the laser process parameters, varying mechanisms responsible for the laser-induced deformation may be active (Fig. 18.2). Vollertsen (1994) first proposed three distinct dominant mechanisms that can be active based upon process parameters as well as material properties and part geometry. These mechanisms were termed: the temperature gradient mechanism (TGM), buckling mechanism (BM) and upsetting mechanism (UM).

The TGM is characterized by a steep through thickness temperature gradient resulting in non-uniform thickness expansion and bending. The vast majority of investigations have focused on LF processes employing this mechanism. As opposed to the TGM which relies on a steep through thickness temperature gradient, operating via the BM results in an almost constant temperature through the thickness, and thus uniform lateral expansion. The surrounding relatively "cold" material acts to constrain the expansion and results in local sheet buckling. Additionally, although the BM is an effective means for generating deformation, it is based upon buckling, an inherently unstable process and thus predicting the bending direction is not

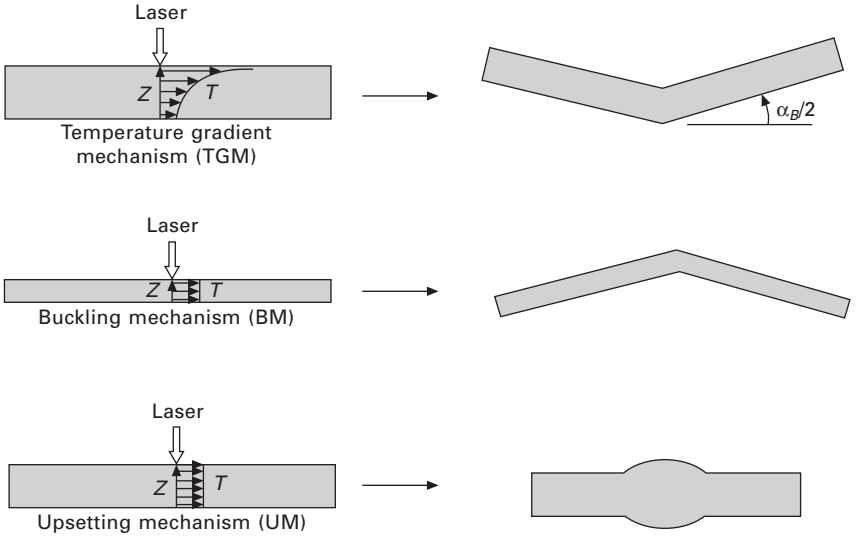

18.2 Schematic of the: (a) temperature gradient mechanism (TGM), (b) bending mechanism (BM), (c) upsetting mechanism (UM).

a straightforward task. However, Li and Yao (2001b) did develop process procedures that result in reliable final deformation. Finally, the UM is also characterized a near uniform temperature distribution through the thickness. However, it seems that this mechanism takes over when the sheet's mechanical properties as well as geometry do not allow local buckling, and instead of resulting in bending, the sheet thickness undergoes significant thickening as well as shortening in the lateral direction.

18.3 Advances in understanding

18.3.1 Geometric considerations

In addition to understanding the fundamental mechanisms for deformation and the impact of varying process parameters, work piece geometry, and laser scan path geometry must also be considered when interpreting experimentally observed process-induced deformations.

Edge effects

One major geometric consideration is the presence of so-called edge effects. For example, if the plate being formed were of infinite length then both the temperature distribution and local mechanical constraints do not vary with respect to a translating coordinate system attached to the moving heat source, satisfying quasi-static conditions. However, operating in close proximity to

traction free surfaces such as when a free edge is approached upon the start and end of straight line scans results in a breakdown of the quasi-static thermal and mechanical conditions. Magee *et al.* (1997) investigated the effects of free edges on the resulting bending angle distribution along the laser scan direction. That work noted that while significant variation of the bending angle occurs (Fig. 18.3), the nature of the variation varies with process parameters as well as the material being formed. For example, they report that in forming pure titanium plates, the bending angle varies non-monotonically with the maximum bending angle occurring near the center of the scan, while for low velocity scans of an AlCuMg alloy, the bending angle increases monotonically from the beginning to the end of the scan. This is explained by sighting the fact that the aluminum alloy has a significantly higher thermal conductivity coefficient, and thus the heat conducted ahead of the source is much greater, acting to decrease the flow stress prior to the heat source arrival thus increasing the plastic strain and final deformation. Bao and Yao (2001) further investigated the effects of the presence of these traction free boundaries and performed a comprehensive investigation on the effects of process parameter variation.

Birnbaum *et al.* (2007), in investigating the effects of work piece clamping also addressed the effects of forming in close proximity to free edges, although their focus was on processing configurations that resulted in scan paths *parallel* to free edges as opposed to the work done by Magee *et al.* (1997) and Bao and Yao (2001) which both analyzed effects stemming from approaching free edges perpendicular to scan paths. They revealed that

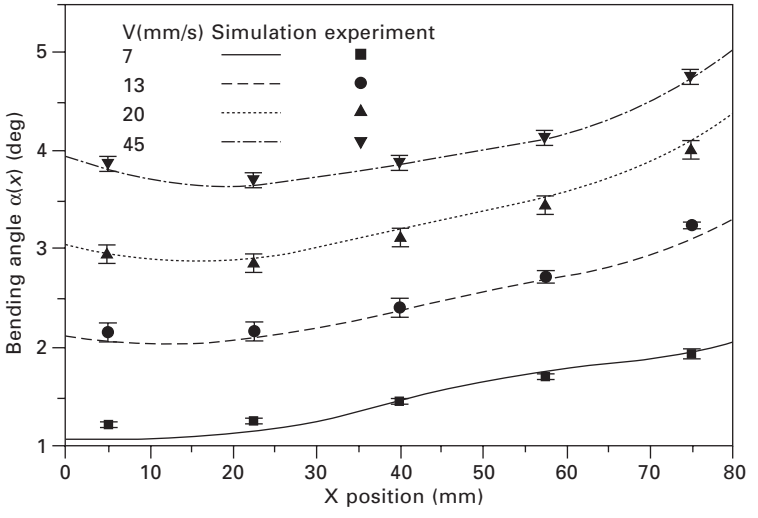

18.3 Bending angle variation along laser scan path (*x*-dir.) due to the presence of free edges perpendicular to the scanning direction (Bao and Yao, 2001).

somewhat counter intuitively, the actual type of clamping constraint utilized had a far less significant effect on the final deformation as compared with the proximity, *'a'* (see Fig. 18.1) with which the laser scan is defined relative to a clamped or traction free boundary.

Three distinct regimes process regimes were identified. As the distance from a free edge (parallel) is approached, the condition goes from one that is basically semi-infinite, to one where the free edge starts to be "felt" in a mechanical sense. Approaching even closer will eventually cause the free edge to be "felt" in a thermal and mechanical sense. For both cases the free edge acts to perturb the symmetric temperature and stress distribution about the heat source. It was revealed that the average bending angle produced was a monotonically decreasing function of the parallel offset distance. This is due to the fact that for the semi-infinite case (far from any free edge), the surrounding relatively "cold" material provides a significant amount of inherent constraint giving rise to large plastic strains perpendicular to the laser travel, and thus large bending angles. However, as a traction-free boundary is approached, the surrounding material, instead of providing a rigid constraint is now able to expand much more freely reducing the magnitude of plastic strain, and thus a smaller bending angle.

Tube bending

The geometry of the work piece itself has also been the subject of several investigations including work by Cheng *et al*. (2005) which studied plate size effects and Cheng *et al*. (2006a) which examined the implications of forming parts with variable thicknesses which was relevant for forming more complex geometries such as the ones presented by air foil compressor turbine blades. A significant amount of work has also gone into process analysis of cylindrical geometries (Fig. 18.4(a) and (b)) for tube and pipe forming. Li and Yao (2001a) propose an analytical model for circumferential scan induced bending deformation in tubes while Zhang *et al*. (2006) examined the effect of the processing scheme in terms of laser beam shape (point vs. line) and whether the scanning is performed axially or circumferentially.

In addition to examining the overall macroscopic deformation of tubes in terms of bending angle, details of the nature of the deformation in terms of local distortions were also investigated. Specifically, Li and Yao (2001a) analyzed wall thickness variation and ovalization as well as changes in the intrados (inner bending surface) and extrados (outer bending surface).

D forming: process design and synthesis

In addition to laser forming rectangular plates, there have been a number of investigations focusing on more complex, three-dimensional geometries.

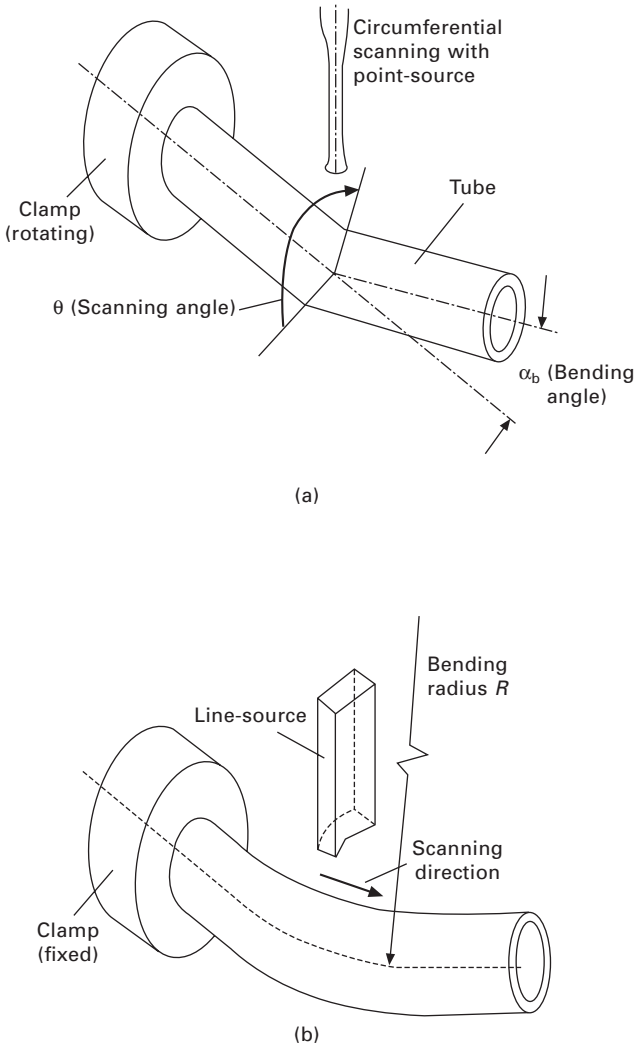

18.4 Tube bending: (a) with circumferential scanning scheme by a point laser source, and (b) with axial scanning by a line laser source (Zhang *et al.*, 2006).

Cheng *et al*. (2006b) examined the implication for forming steel plates of non-uniform thickness. This choice of geometry was made as a first step toward analyzing extremely complex three-dimensional parts such as turbine blades for jet engine compressors. The resulting bending deformation in terms of average bending angle as well as bending angle distribution along the laser scan path was significantly altered as compared to the uniform thickness counterpart (Fig. 18.5). Furthermore, analytical solutions for a plate of varying thickness were also developed.

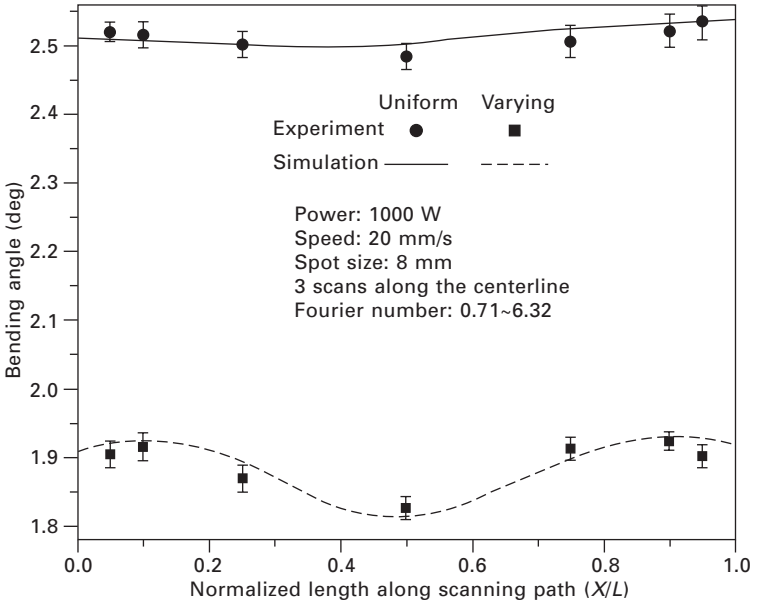

18.5 Bending angle variation of varying thickness plate and uniform-thickness (s_0 = 2 mm) plate along the scanning direction (Cheng *et al.,* 2006a).

A significant amount of effort has gone into simulation and prediction of formed geometry based upon the initial part geometry and processing conditions. However, the so-called inverse problem; that is the ability to determine the necessary process parameters for producing a desired final geometry, is far more industrially relevant. Liu *et al*. (2004) developed a strain-based approach for determining the appropriate laser path geometries for producing pre-conceived doubly curved formed geometries (pillow and saddle). In addition to laser path planning, they also developed a technique for predicting the required heating conditions as well as the path sequence. Zhang *et al*. (2006) utilized this technique applying it to shape tuning of nickel-super alloy airfoils. The geometric deviations between the as-forged and desired shapes can be eliminated by laser forming if as it can potentially provide a more robust, quicker and cheaper than alternative to current methods provided the process does not have any adverse material effects. This work implemented an iterative corrective scheme (Fig. 18.6) which consisted of characterization of the part, and then implementation of the correction scheme for producing the desired geometry. This process was repeated until the formed part was within the desired tolerances.

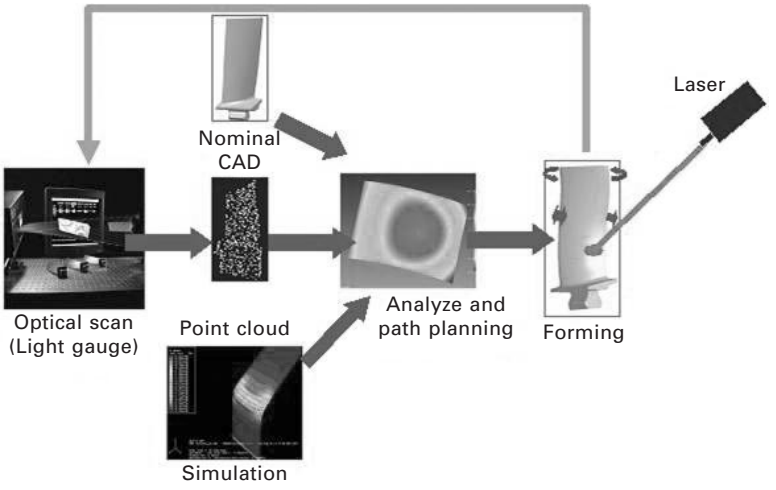

18.6 Strategy for blade shape tuning (Zhang *et al.*, 2006).

18.3.2 Microstructual implications

Anisotropy

In addition to process parameters, geometry and macroscopic material properties, a significant amount of effort has gone into investigating the effects of both the pre-processed microstructure, as well as microstructural modifications induced by the LF process itself. As the LF process results in both thermal and mechanical cycling, particularly for multiple scan cases, the process can result in significant recovery and recrystallization as well as phase transformation (Cheng and Yao, 2002). Cheng and Yao (2005) investigated the effects of rolling induced sheet metal anisotropy in cold-rolled AISI 1010 steel sheets (Plate XVI (a) (between pages 428 and 429) on the resulting process induced deformation. That investigation included an examination of both the extent of the rolling reduction as well as the manner with which the laser scan path is oriented relative to the rolling direction (RD) axis (Plate XVI(b).

Phase transformation and microstructural evolution

In addition to process parameters, geometry and macroscopic material properties, a significant amount of effort has gone into investigating the effects of both the pre-processed microstructure, as well as microstructural modifications induced by the LF process itself. As the LF process results in both thermal and mechanical cycling, particularly for multiple scan cases, the process can result in significant recovery and recrystallization as well as phase transformation (Cheng and Yao, 2002).

Cheng and Yao (2002) observed the maiden ferrite, with some pearlite structures for a low carbon AISI 1012 steel transform to martensite and accompanied by a grain refinement within the heat affected zone (HAZ) thus having undergone dynamic recrystallization.

Fan *et al*. (2005) examined the LF process and its implications for phase transformations in Ti-6Al-4V (Fig. 18.7). That effort demonstrated that for an alloy consisting of an $\alpha + \beta$ phase mixture, that upon heating the alloy transforms completely to β (through the $\alpha \rightarrow \beta$ transformation), and due to the non-equilibrium cooling undergoes a displacement-based martensitic transformation forming an α' martensite. This resulted in a distribution of phase content where within the HAZ, the material consisted of a mixture of mostly α' and some retained β, whereas moving further away from the HAZ, where the cooling rate was not as high, someα returned from a diffusion controlled $\beta \rightarrow \alpha$ transformation. Merklen *et al*. (2001) examined process-induced effects for aluminum and an AlMgSi alloy. In addition to sub-grain structural modifications such as dislocation generation and motion, they

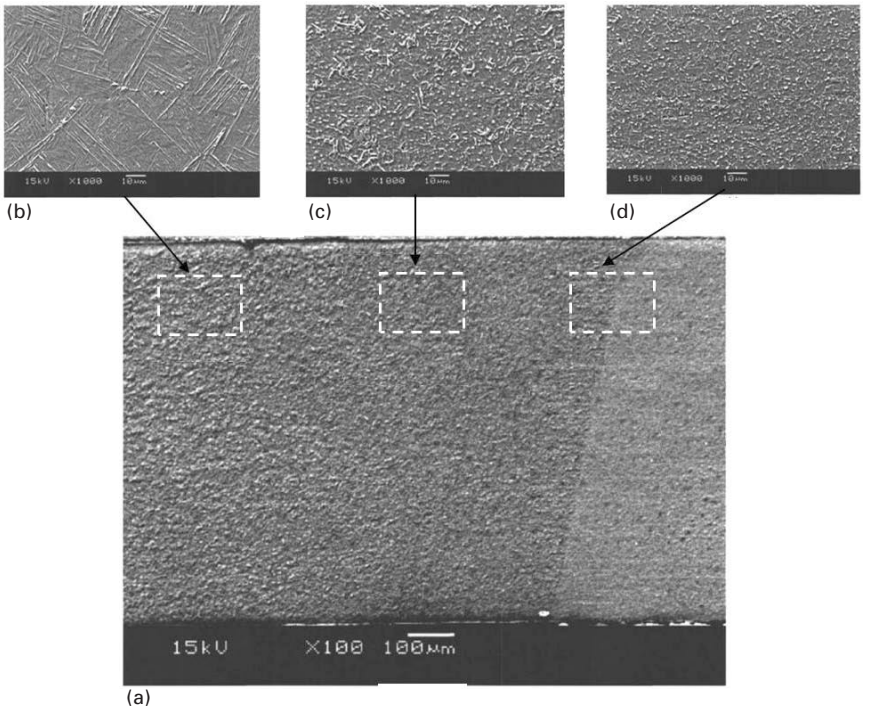

18.7 (a) SEM images of the cross-section perpendicular to the scanning path (P = 1000 W, v = 60 mm/s). (b) close to the scanning path heat source, (c) far from the scanning path, and (d) further from the scanning path, and close to the HAZ boundary (Fan *et al.*, 2005).

also observed the formation of $MgSi_2$ precipitates in the above mentioned alloy.

Birnbaum and Yao (2006) also examined issues associated with laser forming austenitic nickel-titanium (NiTi) shape memory alloys. Specifically, in terms of microstructural modification, they observed that for an initially austenitic plate, the post-process residual stress field induced by LF results in a local *stress* induced phase transformation (Fig. 18.8). Additionally, it is seen that the volume fraction of stress-induced martensite (SIM) is affected both by process parameters and the number of laser scans (Fig. 18.9).

Besides the ability to form parts with desired final geometries, the laser forming (LF) process has recently been shown to have potential as a means for training the two-way shape memory effect (Ostendorf *et al*., 2004). The two-way shape memory effect is characterized by a material's ability to "remember" two distinct configurations. Ostendorf *et al*. (2004) showed that through multiple pulsed laser forming of NiTi thin foils, one could "train" the formed part to have two distinct configurations that may be activated solely by thermal means.

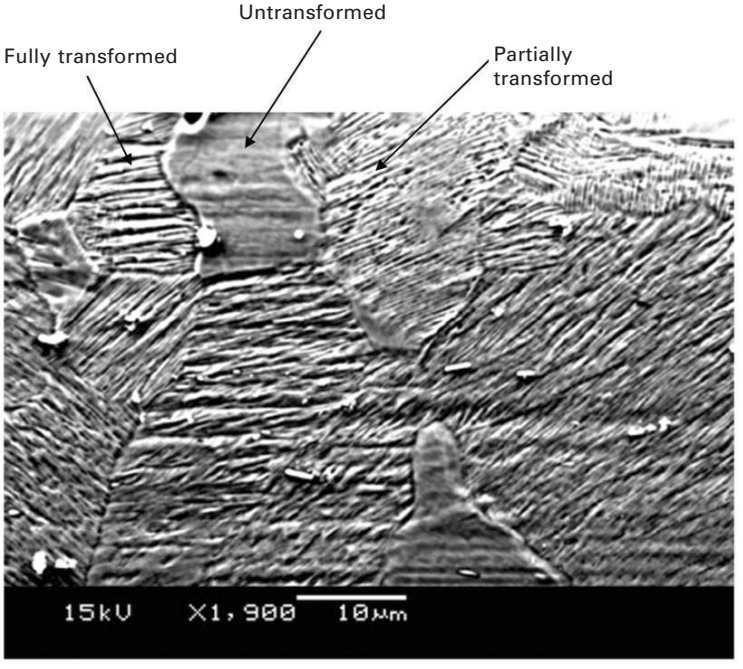

18.8 Micrograph of through thickness cross-section of five scan specimen (high magnification, top surface). Note the presence of grains of varying extent of transformation (P = 250 W, v = 15 mm/s, d = 7 mm). (Birnbaum and Yao, 2006).

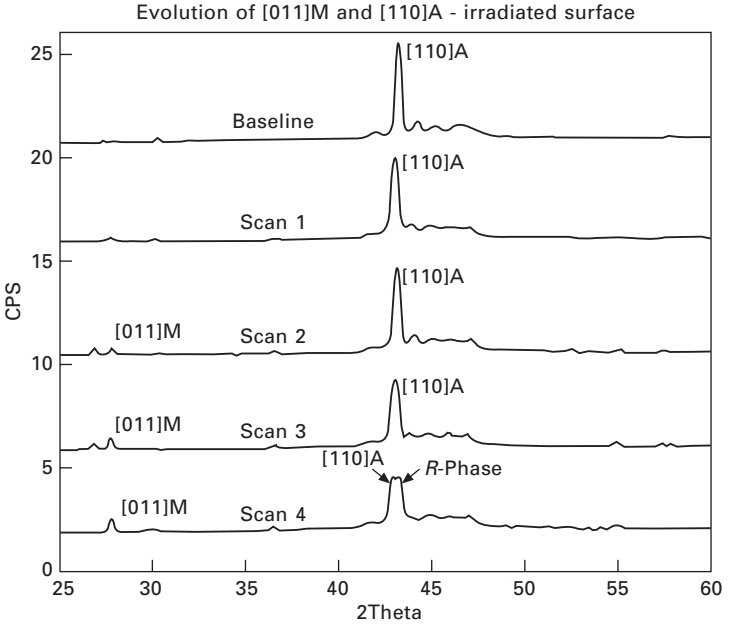

18.9 X-ray diffraction spectra over successive scans (P = 250 W, v = 15 mm/s, d = 7 mm) revealing an increase in martensitic content at the expense of the parent austenitic matrix (irradiated surface). Note the presence of R-phase in the fourth scan (A - Austenite, M - Martensite). Also note the negative peak shift from the baseline corresponding to compressive residual stress (Y-direction) in the irradiated surface (Birnbaum and Yao, 2006).

Numerical simulation: phase transformation and microstructural evolution

In addition to experimental observations of the microstructure resulting from having undergone the laser forming process, a number of efforts have gone into simulation and prediction utilizing a number of numerical techniques. Techniques for integrating these microstructural changes into predictions for simulating the resulting mechanics of the laser forming process have also been developed. Cheng and Yao (2002) utilized an iterative scheme for multiple scan forming processes (Fig. 18.10) which determined characteristics regarding dynamic recovery and recrystallization and calculated changes in the volume fraction of the predominantly ferritic (with some pearlite) maiden structure to austenite upon heating, and martensite upon rapid cooling. Diffusional transformations were modeled using a JMAK kinetics approach, while diffusionless (martensitic) transformations were performed via the implementation of an Arrhenius-like approach. These changes in volume fraction to the respective phases are then utilized for

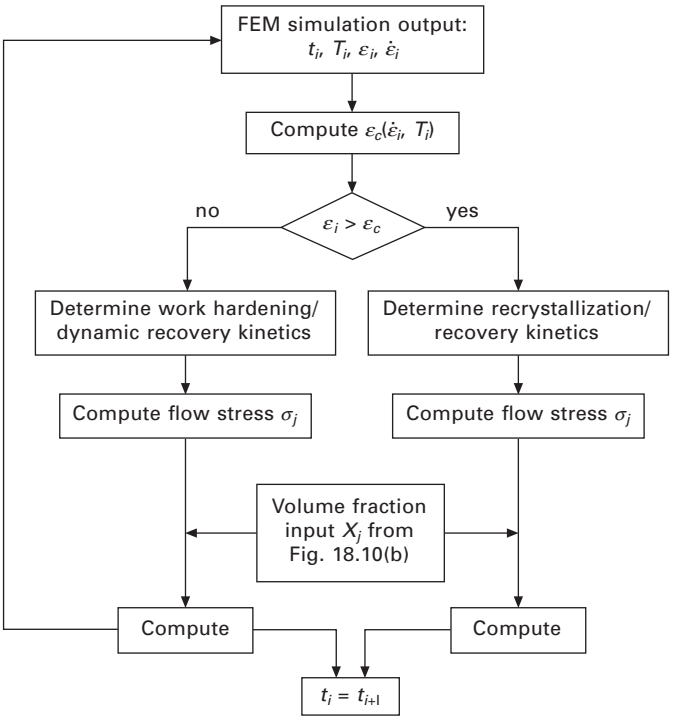

18.10 Algorithm for (a) recover/recrystallization, and (b) phase transformation constitutive modeling (index *j* denotes the *j* th phase). (Cheng and Yao, 2002).

updating material properties such as Young's modulus and flow stress as a function of temperature for determining the deformation. Furthermore, these microstructural inhomogeneities are then stored as initial conditions for modeling subsequent laser scans.

Approaches for modeling grain refinement due to dynamic recovery and recrystallization were also investigated. Fan *et al*. (2005) utilized a coupled finite element-monte carlo technique for simulating the grain refinement due to the heating cycle, including contributions from strain energy from thermal expansion induced by the laser treatment (Plate XV between pages 428 and 429).

18.4 Laser shock peening

18.4.1 Historical perspective

Laser shock peening (LSP) is a process that was developed as a substitution for conventional shot peening. It is a surface treatment that is used to improve fatigue life and wear resistance of metallic parts. The process consists of inducing compressive residual stresses into the target material, which as a result impedes crack propagation and increases the lifespan of the metallic components. The LSP process was invented at Battelle Memorial Institute in 1972. Since then it has been studied by many researchers worldwide (Clauer and Holbrook 1981; Peyre *et al*., 1996; Hammersley *et al*., 2000; Zhou *et al*., 2003). The process is mainly used in the aerospace industry for treatment of jet engine turbine blades, which during the take-off and landing are subject to foreign object damage as stones and ice are sucked into the engine causing damage to the blades and reducing their service life.

The laser beam spot size in LSP is on the order of millimeters. The high cost of the lasers capable of producing such large size beam spots with intensities of several GW/cm^2 prevented wider industrial application of LSP. However, the recent progress in the fabrication of micro electromechanical systems (MEMS) as well as other micron size devices and the use of metallic components within them motivated the development of micro-scale laser shock peening (μLSP). The process was proposed for the first time by Zhang and Yao (2001) who recognized the potential of fatigue life enhancement of metallic micro components through inducing compressive residual stress with spatial resolution in the order of microns. Investigation of μLSP as a technique (Zhang and Yao, 2002; Chen *et al*. 2004a,b) included potential improvement of micro parts that undergo cyclic loading during their service time such as MEMS actuators, medical implants, micro-switches, relays and blades of micro impellers.

Physical description of process

Laser shock peening is accomplished as laser pulses focused on the top surface vaporize an ablative layer, usually black paint or thin metallic foil, creating hot plasma whose expansion induces shock waves into the target material. High amplitude pressure pulses are formed in the following way. When a laser beam with sufficient intensity strikes the surface, a thin layer of material is vaporized. Due to rapid energy deposition, the affected region is confined to a small area as thermal diffusion out of the interaction zone is limited. The temperature of the vaporized material rises quickly, achieving values of several tens of thousands of degrees (Clauer and Holbrook, 1981) resulting in ionization and subsequent plasma creation. Newly created plasma continues to absorb laser energy until the end of the pulse duration. Plasma is characterized by high pressure (1–10 GPa) and high temperature, and its hydrodynamic expansion is responsible for the shock wave propagation. The magnitude of the pressure increases by a factor of five or more if the plasma is confined by an overlay transparent to the laser wavelength as compared to unconfined, i.e. open air, conditions because confining medium impedes plasma expansion in the direction opposite of the target material (Zhang and Yao, 2002). In addition, the shock pressure duration is two to three times longer than the laser pulse itself if the plasma is covered with confined medium. The LSP process is schematically depicted in Fig. 18.11.

The process is assumed to be adiabatic and therefore the target material is only subject to mechanical loading, due to the fact that the coating is just partially ablated where the remaining portion serves as a shield to thermal influence. The load is applied as a short impulse and it propagates as a shock wave, plastically deforming the material.

Fatigue performance enhancement through micro-scale laser shock peening

Advantages of the micro-scale laser shock peening (μLSP) over the LSP process is that it does not require high-energy laser systems utilized in LSP, reducing the overall cost of the process. Further, the spot size is in the order of microns, and therefore intensities are comparable to those in LSP and yet laser pulses are delivered at higher repetition rate. Small spot size also allows greater flexibility in treatment of micro devices, where μLSP can be used selectively to treat only regions around stress concentration points. On the other hand, LSP induces compressive residual stresses up to 400 MPa and up to 1 millimeter depth (Clauer and Holbrook, 1981), whereas the μLSP induces compressive residual stresses about half or an order of magnitude smaller than induced by millimeter-scale LSP and up to tens of microns deep (Zhang and Yao, 2002). Zhang and Yao (2001) performed fatigue testing on the scaled down copper dog bone specimen, previously treated with μLSP.

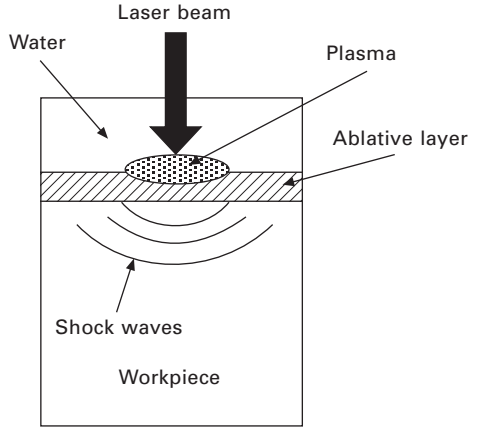

18.11 Schematic of the laser shock peening process.

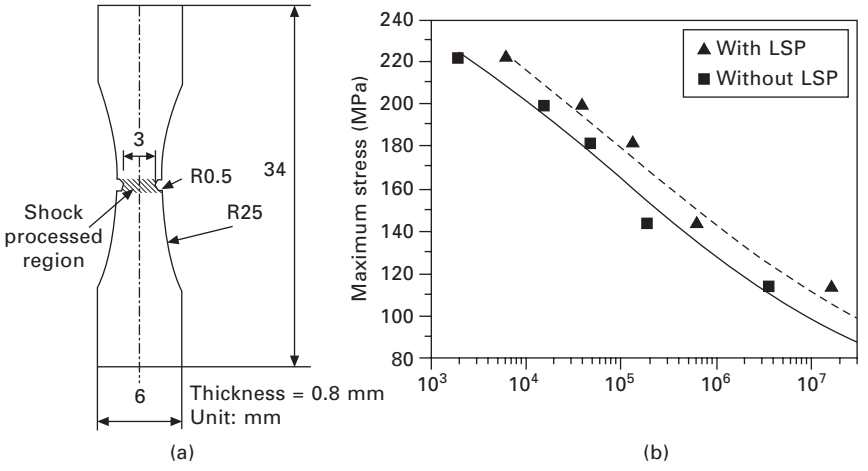

18.12 (a) Geometry of fatigue test sample (b) fatigue test results. The dotted region near the notches is laser shock processed by applying laser pulses along the width direction with uniform spacing between pulses of 50 microns, three pulses at each location, pulse energy E = 220 μJ. The lines in (b) are least-square fitted curves of the experimental results. Scale is logarithmic (Zhang and Yao, 2001).

Results have shown (Fig. 18.12) that fatigue life of a treated specimen is three times longer than the control one (Zhang and Yao, 2001).

18.4.2 Anisotropic and Heterogeneous Response

The laser beam spot size in micro-scale laser shock peening (μLSP) is usually several microns in diameter and thus about the same order of magnitude of

average grain size of most polycrystalline materials used in fabrication of micro devices (aluminum, copper, etc). Few grains at most are actually affected by a single laser pulse. Therefore the effects of anisotropy and heterogeneity have to be taken into account to properly understand this process.

Anisotropic response

Effects of anisotropy under micro-scale laser shock peening have been studied in aluminum single crystals subject to plane strain conditions (Chen *et al*., 2004a, 2004b; Wang *et al*., 2008b; Vukelic *et al*., 2008a, 2008b). Various aspects of material response to the pressure load have been investigated experimentally and theoretically including residual stress deformation, crystallographic lattice rotation and distribution of the plastic deformation

Residual stress distribution

The residual stress measurement in single crystal aluminum after μLSP processing has been characterized utilizing x-ray microdiffraction (Chen *et al*., 2004a; Vukelic *et al*., 2008b). Chen *et al*. (2004a) utilized synchrotron radiation source and implemented a method developed by Ungar to characterize residual stress induced by μLSP in single crystal aluminum, subject to plane strain condition.

If a piece of metal is deformed elastically such that the strain is uniform over a relatively large distance, the uniform macro-strain will cause a shift in the x-ray diffraction lines to new positions. If the metal is deformed plastically, the deformation creates adjacent regions of slight different orientations. The residual strain can vary from region to region to cause nonhomogeneous strain state, which causes a broadening of the x-ray diffraction profile. In fact, both kinds of strain are superposed in plastically deformed metals, and diffraction is both shifted and broadened (Cullity, 1978). On the basis of a composite model, local strain and residual stress can be evaluated for single crystal metal under plastic deformation as reported by Ungar *et al*. (1984) by recognizing that the crystal dislocations often arrange themselves in a cell structure. In the model, the deformed crystal is considered as a two-component system, where the local flow stress of the cell walls is considerably larger than the local flow stress of the cell interiors. Consequently, in the plastically deformed and unloaded crystals the cell walls parallel to the compressive axis are under a residual uniaxial compressive stress and the cell interior under a uniaxial tensile stress. The asymmetrical Bragg reflections can be separated into the sum of two symmetrical peaks which correspond to "cell interiors" and "cell wall" as seen in Fig. 18.13. The integral intensities of the sub-profiles relative to the integral intensity of the measured profile are proportional to the volume fractions of the cell walls, and cell interiors,

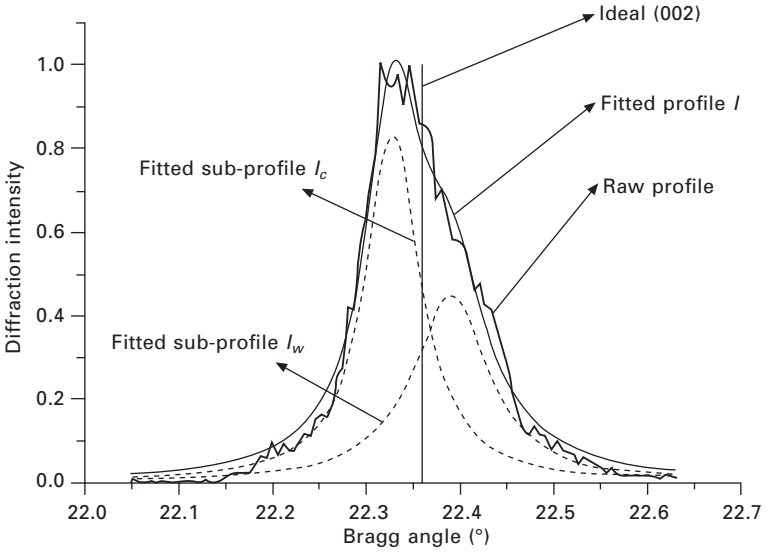

18.13 Detailed view of decomposition of an asymmetric line profile into the sum of two symmetric sub-profiles, diffraction intensity normalized (sub profile I_c: cell interior; and sub profile I_w: cell wall) (Chen *et al.*, 2004a).

respectively. The asymmetric line profiles I are assumed to be composed of two components I_w and I_c, where I_w is attributed to the cell-wall and I_c to the cell-interior. The centers of both components are shifted in opposite directions. These shifts express the relative change of the mean lattice plane spacing. Further, the measure of the residual stress is characterized as absolute value of the difference between stresses corresponding to cell walls and cell interiors. Residual stress distribution in aluminum single crystal with (110) surface orientation is shown in Fig. 18.14.

Single crystal plasticity and crystallographic lattice rotation

According to the single crystal micromechanics (Asaro, 1983) the deformation gradient tensor, F, which governs the plastic deformation in single crystals can be conceptually broken down into three steps, which when combined together determine the overall deformation gradient F: first plastic slip through the undeformed crystal F^P, second rigid body rotation F^R, and finally elastic stretching of the lattice F^e. The first two terms can be combined together and the general expression for deformation gradient becomes $F = F^* \cdot F^P$, where F^P is deformation related to the plastic shear and F^* represents stretching and rotation of the crystal lattice.

This approach has been adopted by Chen *et al.* (2004b) and followed by

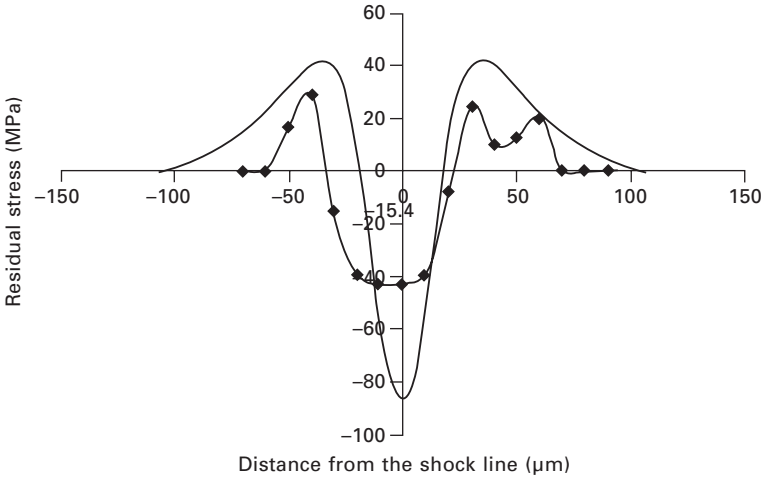

18.14 Residual stress measured via x-ray microdiffraction. Experimental and numerical results are superimposed for comparison purposes (Vukelic *et al.*, 2008b).

Wang *et al*. (2008a) and Vukelic *et al*. (2008a; 2008b) to describe plastic deformation in single crystals induced by μLSP process and anisotropic behavior that stems from it. Closed form solution for the stress and deformation field for aluminum with $(1\bar{1}4)$ orientation of its top surface has been obtained by Wang *et al*. (2008a) approximating loading from the μLSP as a punch with non-uniform pressure distribution (Fig. 18.15(a), Table 18.1(a)). Solution is achieved utilizing anisotropic slip line theory (Booker and Davis 1972; Rice 1973), assuming equilibrium conditions, plane strain deformation state and rigid ideally plastic material. The plane strain condition in face centered cubic (FCC) crystals is achieved when loading is applied along (110) direction (Rice 1987). In that case out of a total of twelve slip systems present, three pairs act cooperatively to create their active in-planes slip systems. Stress and deformation field for the (110) orientation and comparison against $(1\bar{1}4)$ orientation has been done by Vukelic *et al*. (2008a), (Fig. 18.15(b), Table 18.1(b)).

In single crystals subject to plane strain deformation state lattice rotation can be characterized experimentally by comparing the as-deformed crystallographic orientation obtained through a mapping of the in-plane rotation of the crystalline lattice (Kysar *et al*., 2005) to the known undeformed state. As a consequence angle of in-plane lattice rotation of the crystallographic lattice can be calculated. Rotation of lattice due to μLSP can be characterized by means of the electron back scatter diffraction (EBSD) measurements.

The mapping of the lattice rotation of the top surface of aluminum $(1\bar{1}4)$ and (110) orientations via EBSD is shown in Plate XVII (between pages 428

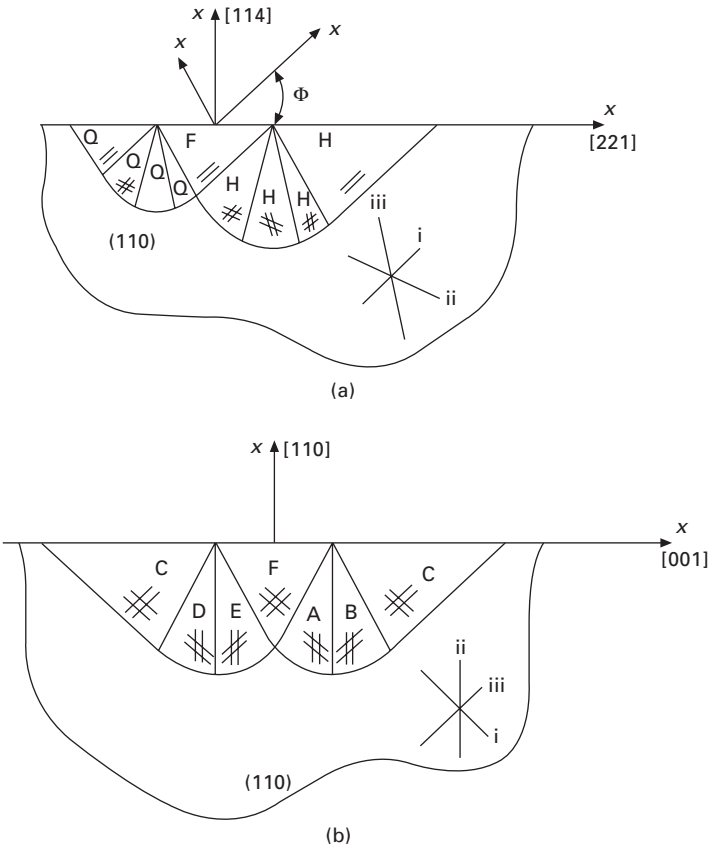

18.15 Geometry of slip line field under Gaussian loading (a) $(1\bar{1}4)$ orientation (Wang *et al.*, 2008b); (b) (110) orientation (Vukelic *et al.*, 2008a). Sectors represent areas of constant stress and correspond to the vertices of the yield surfaces constructed utilizing anisotropic slip line theory and following principles of Rice (1973; 1987).

and 429). Rotation about the shock line center is anti-symmetric, the blue region corresponds to counterclockwise rotation (CCW), and the red region corresponds to clockwise rotation (CW). Deformation is largely uniform along the shock line on the treated surface, which indicates an approximate two-dimensional deformation state is achieved by shocking the single crystal along the (110) direction which is in good agreement with theoretical predictions of Rice (1973; 1987). Further, in-plane lattice rotation in cross-section is depicted in Plate XVIII (between pages 428 and 429) where it can be seen that rotation in (110) case is almost twice the rotation for the $(1\bar{1}4)$ case which is consistent with analytical predictions of Vukelic *et al.* (2008a).

Table 18.1 (a) Stresses within sectors ($1\bar{1}4$) case, (b) Stresses within sectors (110) case

Sector	σ_{11}/τ_{cr}	σ_{22}/τ_{cr}	σ_{12}/τ_{cr}	Active slip
(a) H	$-\sqrt{6}$	0	0	*i*
H_1	$-\frac{11}{9}\sqrt{6}$	$-\frac{4}{9}\sqrt{6}$	$-\frac{4}{9}\sqrt{3}$	*i* & *iii*
H_2	$-\frac{4}{3}\sqrt{6}$	$-\frac{11}{6}\sqrt{6}$	$\sqrt{3}$	*ii* & *iii*
H_3	$-\frac{13}{9}\sqrt{6}$	$-\frac{49}{18}\sqrt{6}$	$\frac{5}{9}\sqrt{3}$	*i* & *ii*
Q_3	$-\frac{16}{9}\sqrt{6}$	$-\frac{23}{9}\sqrt{6}$	$-\frac{4}{9}\sqrt{3}$	*i* & *iii*
Q_2	$-\frac{5}{3}\sqrt{6}$	$-\frac{7}{6}\sqrt{6}$	$-\sqrt{3}$	*ii* & *iii*
Q_1	$-\frac{14}{9}\sqrt{6}$	$-\frac{5}{18}\sqrt{6}$	$-\frac{5}{9}\sqrt{3}$	*i* & *ii*
Q	$-\sqrt{6}$	0	0	*i*
(b) A	$-\frac{3}{2}\sqrt{6}$	$-2\sqrt{6}$	$-\sqrt{3}$	*i* & *ii*
B	$-\frac{3}{2}\sqrt{6}$	$-\sqrt{6}$	$-\sqrt{3}$	*ii* & *iii*
C	$-\sqrt{6}$	0	0	*i* & *iii*
D	$-\frac{3}{2}\sqrt{6}$	$-\sqrt{6}$	$-\sqrt{3}$	*i* & *ii*
E	$-\frac{3}{2}\sqrt{6}$	$-2\sqrt{6}$	$-\sqrt{3}$	*ii* & *iii*

Predictive capabilities

The nature of the micro-scale laser shock peening (μLSP) process is highly dynamic. However, finite element models used to develop predictive capabilities in μLSP were focused on the anisotropic response did not take into account inertia (Chen *et al*., 2004b; Wang *et al*., 2008a). These models utilized crystal plasticity theory developed by Hill (1950), Rice (1973; 1987), Asaro (1983) and Asaro and Needleman (1985). Obtained results were in good agreement with analytical predictions obtained using anisotropic slip line theory. On the other hand, material response under dynamic loading has been studied as shock wave propagation in isotropic materials under LSP (Peyre *et al*., 2003) and μLSP (Fan *et al*., 2005). Single crystal plasticity was combined with dynamic loading by Nemat-Nasser *et al*. (1998) through study of dynamic void collapse. Vukelic *et al*. (2008b) incorporated single crystal plasticity and work hardening model of Pierce *et al*. with dynamic loading in μLSP finite element model.

Propagation of the elastic precursor wave that precedes plastic deformation under the μLSP process is analogous to the elastic propagation of waves,

used in non-destructive evaluation (NDE) for calculation of ultrasonic field profiles in mildly anisotropic media. This approach considers wave propagation from a finite-sized transducer source which is equivalent to the compressive surface traction induced by Gaussian pressure distribution. The basis for the NDE is Huygen's principle and retarded potentials based on the existence and properties of the temporal Fourier transformation of the Green's function. Tverdokhlebov and Rose (1988) employing the Helmholtz decomposition, represented the Green's function as a sum of three components corresponding to plane wave propagation of quasi-longitudinal and two quasi-transverse velocities present in the arbitrary anisotropic, homogeneous solid. Numerical integration of the Green's function presented by Rose *et al*. (1989) as an output gives elastic wave velocity profiles for quasi-longitudinal and two quasi-transverse wave modes. These transducer field profiles in essence represent strain energy density and from them it can clearly be seen that deformation propagates in the direction of the applied load without little lateral expansion beyond boundaries of the source. In the case of the μLSP this effect is observed through examination of total shear at the end of the loading, shown in plate XIX (between pages 428 and 429). It appears that plastic deformation occurs predominantly under the Gaussian pressure load for both, $(1\bar{1}4)$ and (110) crystal orientation. In addition, another important consequence of anisotropy should be noted: direction. The wavefront normal vector does not coincide with wave velocity vector for an anisotropic medium. This leads to the skewing of the direction of the strain energy density propagation in the direction of large phase velocity, resulting in the asymmetric material response. Plastic deformation propagates in the direction of the longitudinal axis of symmetry of yield loci showing that symmetric and asymmetric yield surfaces produce symmetric and asymmetric plastic deformation. The numerical results are in very good agreement with experimental findings. In Fig. 18.14 experimental findings for residual stress for the aluminum of (110) orientation are superimposed with numerical results, which represent the weighted average of the residual stress in horizontal direction. Weight function is chosen such that takes into account fractional contribution of progressively deeper layers to the diffracted intensity (Noyan and Cohen, 1987). Both, numerical values and trend of stress distribution is consistent with experimental measurements, showing that stresses near to surface in region close to the shock line are mostly compressive, which is beneficial for improvement of fatigue life of micro components. In addition, superimposed experimental and numerical values for displacement for both (110) and $(1\bar{1}4)$ crystal orientation are shown in Fig. 18.16. Also cross-sectional contour maps of the lattice rotation for these two crystallographic orientations are depicted in plate XX(a) and (b).

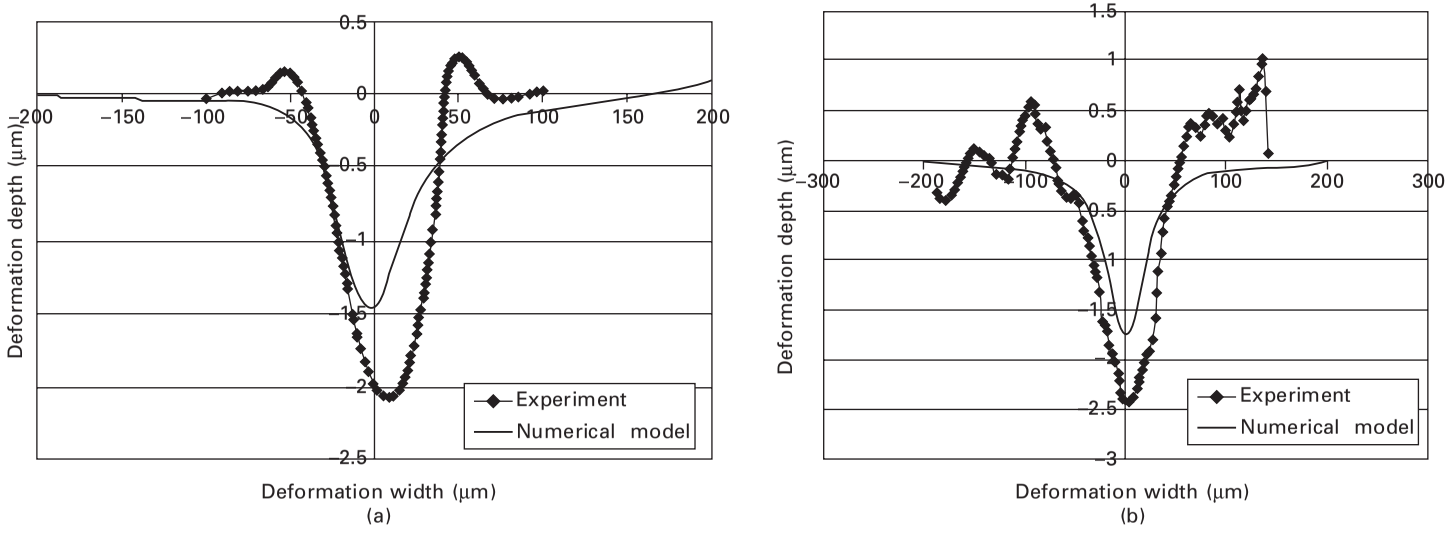

18.16 Deformation field measured via profilometer and AFM, respectively (a) orientation (1$\bar{1}$4) (b) orientation (110).

Effects of heterogeneity

An effect of heterogeneity under micro-scale laser shock peening (μLSP) is studied in aluminum bicrystals (Vukelic *et al.*, 2008c). Orientations of crystals in bicrystal are chosen such that if laser shocks are applied along the grain boundary, both crystals will experience plane strain deformation. Heterogeneity has been studied experimentally and numerically. The finite element model has been developed in which bicrystal is decomposed into grain interior simulated utilizing single crystal plasticity and grain boundary. The grain boundary is assumed to be rigid, neither debonding nor sliding is allowed to occur. Such an assumption discounts the potential of grain boundary deformation. However, since the applied loads on the grain boundary are highly compressive, no debonding is expected to occur.

Figure 18.17 shows the geometric profile at the grain boundary from the profilometer measurements and in the reference single crystals after shocking. It can be observed that depth of deformation close to the grain boundary is smaller than in reference single crystals. Numerical results for the shear strains on each active in-plane slip system are shown in plate XXI (a), (b) and (between pages 428 and 429). There is a total of three active in-plane slip systems and they are denoted as *i*, *ii* and *iii*. The total accumulated shear in the aluminum bicrystal, is shown in plate XXI(d). The orientation of crystals in the bicrystal is such that the same slip systems are active and furthermore the yield loci have the same shape and orientation. However, the

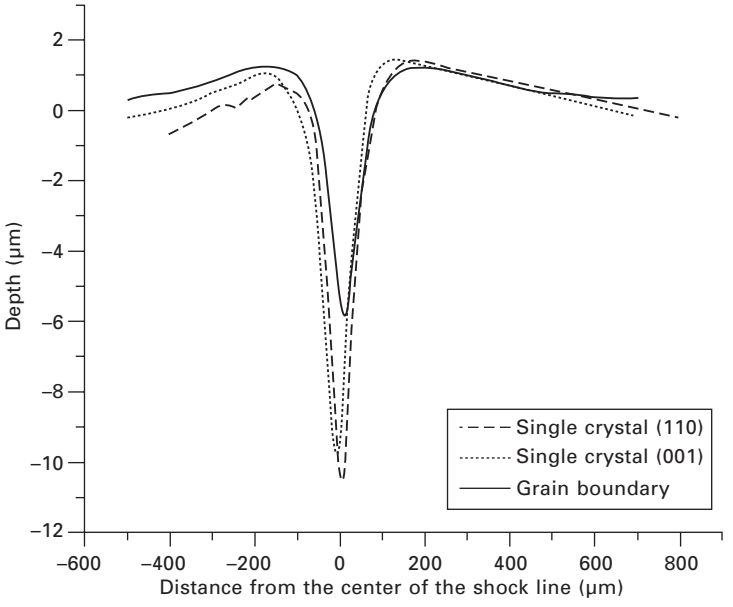

18.17 Deformation geometry after shocking (a) experimental results.

domain of interest is asymmetric due to the presence of the grain boundary, and one would intuitively assume that total shear strain field should indicate a lobe of deformation with higher magnitude in the right crystal where the slip direction does not point into the boundary. This is not the case, however, as will become apparent, the effects of inertia are dominant over anisotropy. Further, it can be seen that the slips on slip systems *i* and *iii* also experience a sharp discontinuity at the grain boundary as seen in plate XXI(a) and (b). The discontinuity is a consequence of an inability of the slip to transmit through grain boundary as well as a sudden change of resolved shear stress at the grain boundary, which introduces an effect analogous to the dislocation motion behavior where dislocations are piled up at the grain boundary. Thus, plastic slip flows under compressive μLSP loading in each crystal until it reaches the grain boundary, which inhibits the plastic slip to be less than would otherwise occur in a single crystal.

18.4.3 Dual-sided micro-scale laser shock peening

Owing to the large pressures involved in laser shock peening (LSP), one-sided laser shock peening on thin targets can result in significant permanent deformation or spall failure on the back surface. Generally, when treating a thin section, opposing dual-sided laser shock peening is used to avoid harmful effects such as spalling and fracture. Opposing dual-sided LSP is accomplished by splitting the laser beam in half and peening opposing surfaces of the target. The pressures on the opposite surfaces of the target balance one another and prohibit excessive deformation of the target. Thus the shock waves from each surface will interact in different ways through the thickness resulting in more complex residual stress profiles.

Numerical modeling is an effective way to understand wave–wave interaction in solids. Mok (1968) simulated the propagation and attenuation of spherical and plane shock waves in a 2024 aluminum plate by assuming that the media is a strain-rate independent and elastic-perfectly plastic solid. Caruso *et al.* (2002) also numerically investigated laser-generated shock propagation dynamics in the solids, but only an elastic medium in plane geometry was considered. Shock-solid interaction was also simulated in some studies of spallation and residual stresses induced by LSP (Cottet and Boustie, 1989); however, the effect of high strain rate was not considered or fully considered only by the Johnson–Cook law. Fan *et al.* (2007) investigated dual-sided micro-scale LSP numerically through development of a finite element model (FEM), in which the hydrodynamic behavior of the isotropic material and the deviatoric behavior including work hardening and strain rate effects were considered. Understanding wave–wave interaction enables optimization of processing conditions through selective modification of the compressive residual stress distribution in controlled manner.

Dual-sided vs single-sided irradiation

Fan *et al*. (2007) addressed the difference in residual stress distribution between dual-sided and one-sided irradiation, as well as the influence of material thickness to enhance understanding of how wave–wave interaction modifies final stress distribution. Two specimen thicknesses are chosen, 100 μm and 200 μm. Figure 18.18 shows the comparison of the top surface average residual stresses distribution between one-sided irradiation and zero-phase dual-sided irradiation. This kind of surface residual stress profile has been reported in literature (Clauer and Lahrman, 2001; Peyre *et al*., 2003; Zhang and Yao, 2000, 2002). From Fig. 18.18, it is found that in zero-phase dual-sided irradiation the top surface compressive residual stresses are higher in magnitude for both 200 and 100 μm thick samples, leading to enhancement of the fatigue life. In zero-phase dual-sided irradiation LSP, the shock wave from the top surface will meet the shock incident from the bottom surface at the midplane and the encountering shock waves will exhibit a constructive interference effect. In this manner, the respective deep compressive residual stress regions that extend from each of the adjacent nonoverlapping laser shock peened surfaces will overlap and significantly increase the peak pressure experienced by the material in the vicinity of the shock wave intersection plane.

Effect of phase on residual stress distributions

Plate XXII (between pages 428 and 429) shows the radial residual stress distributions within the 100 μm thick copper plate by various irradiation methods. From Plate XXII it can be seen that dual-sided irradiations gain a more compressive and wider distributed surface residual stress compared with one-sided irradiation. In dual-sided irradiations with different phases, the compressive surface residual stress profiles are also different: full phase results in the most compressive and widest surface residual stress profiles, and zero-phase obtained the least compressive and narrowest surface residual stress distributions. But with different phases, the depth of penetration of residual stress into surface does not show evident difference. The surface residual stresses in the 200 μm thick sample exhibit similar trends as those seen in the 100 μm thick specimen.

18.5 Laser peen forming

18.5.1 Historical perspective and process description

Laser peen forming (LPF) is a novel process. It combines the beneficial effects of micro-scale laser shock peening with a controlled bending deformation to shape micro-scale metallic parts without hard tooling. By

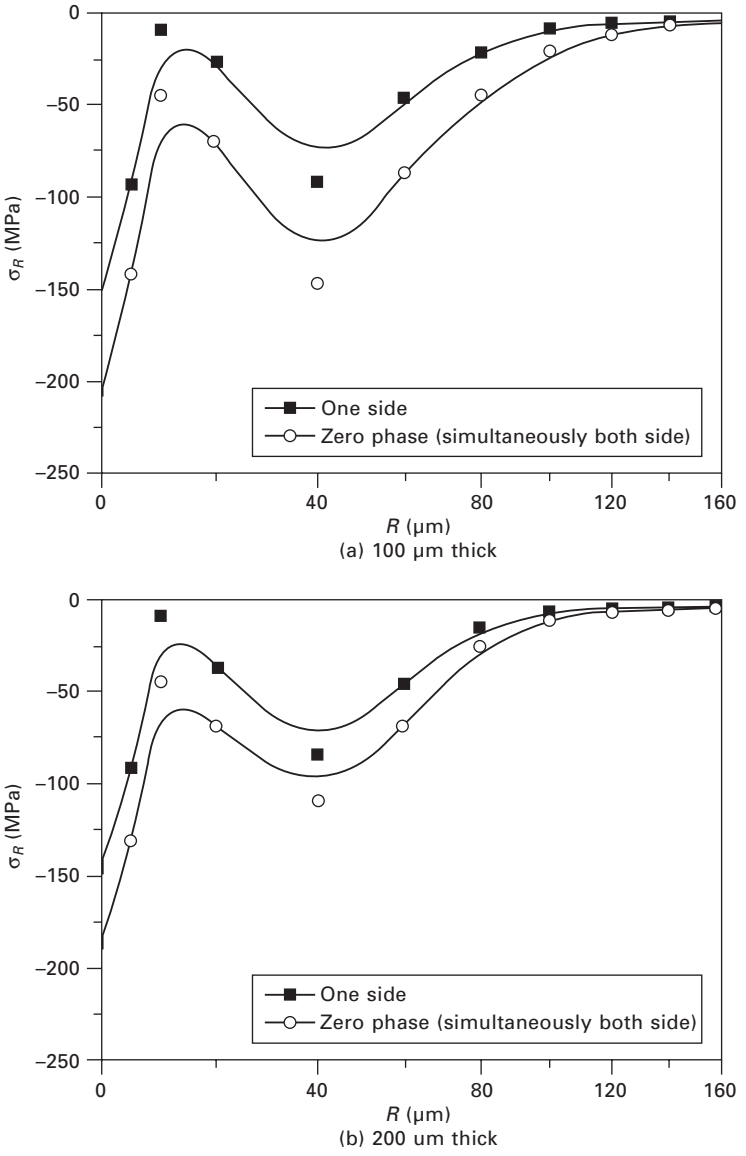

18.18 Comparison of the calculated top surface residual stresses between one-sided irradiation and zero-phase dual-sided irradiation in the samples with different thickness: (a) 100 and (b) 200 μm thick. The horizontal axis represents distance from the center of the laser spot. Laser intensity is 4.95 GW/cm^2, beam spot size is 12 μm, and pulse duration is 50 ns.

matching process conditions with workpiece material, geometry, and boundary conditions, different deformation mechanisms can be invoked to generate rich combinations of desired local and global deformations simultaneously

in a single step. LPF provides process simplicity and flexibility as well as new design opportunities of micro parts. In this method laser shocks are applied onto the surface of the free standing thin metal sheet coated with ablative layer and submerged into the confining medium, similarly to the laser shock peening process. Plastic deformation is induced through shock wave propagation which serves a dual purpose, inducing compressive residual stresses and convex or concave curvature.

Hackel and Harris (2002) employed a pulse laser beam for forming shapes and contours in metal strips. They showed that the LPF process can generate deep compressive stress without inducing unwanted tensile stress at the metal surface and is especially useful for thick material that is difficult to shape or contour. Zhou *et al*. (2002) investigated the deformation mechanisms for a special configuration; that is, a sample clamped by two concentric washers. Laser spot size they used ranges from 3 to 10 mm in diameter. By using LPF, metal sheet forming is realized without mold and the dimensions of the obtained shapes are determined by the boundary condition. Zhou *et al*. (2003) further studied the response of various metal sheets to LPF and presented detailed deformation characterization. The investigation showed its potential to become a flexible manufacturing process with excellent properties and short manufacturing time. Recently, microforming became an important technology for manufacturing micro-metallic parts (Geiger *et al*., 2001; Cao *et al*., 2004). Microforming using laser has already been explored for a number of potential high-precision industrial applications, such as laser microbending of magnetic disk-drive components, adjustment of contact springs of miniature relays and reed contacts, accurate bending of thin plate springs, etc. (Otsu *et al*., 2001; Esser *et al*., 2003). It can be seen that most of these applications encounter cyclic loadings. Thus, it is desirable to improve fatigue life of microparts after the microforming process. Wang *et al*. (2007) showed that compressive residual stress can be induced on both sides of the workpiece, similarly to macro-LPF.

18.5.2 Geometric constraints

Forming process

The global deformation and residual stress pattern in the micro-scale laser peen forming (μLPF) is a function of various parameters, such as laser pulse energy, type and thickness of the target material. Wang *et al*. (2008b) investigated the relationship between the residual stress and forming mechanisms. Study included experimental and numerical aspects and two energy levels 4.95GW/cm^2 and 3.57GW/cm^2, determining the forming mechanism were used.

It is found that at higher laser intensities the stress on the bottom is first tensile to balance the compressive stress of the top surface and then changes to compressive as the specimen bends upward for the 4.95GW/cm^2 laser

intensity (Fig. 18.19(a)). For the case of 3.57GW/cm^2, the tensile residual stress occurs on the treated surface as the bending is reversed. Figure 18.19(b) shows the distribution of averaged stress within 30μm from the top right after the moment of unloading for two energy levels. This demonstrates

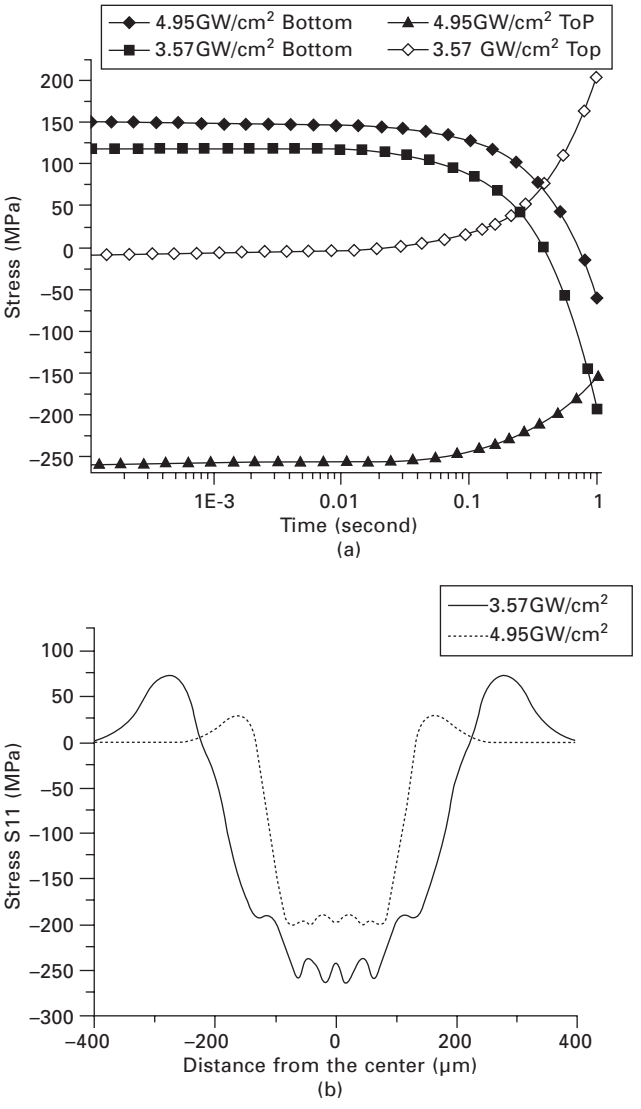

18.19 Stress and wave propagation from FEM: (a) time trace of lateral stress of the central points on both sides of surface (b) spatial distribution of stress on the top surface at the beginning of unloading (c) wave propagation along the surface direction on the top surface (d) wave propagation in depth direction.

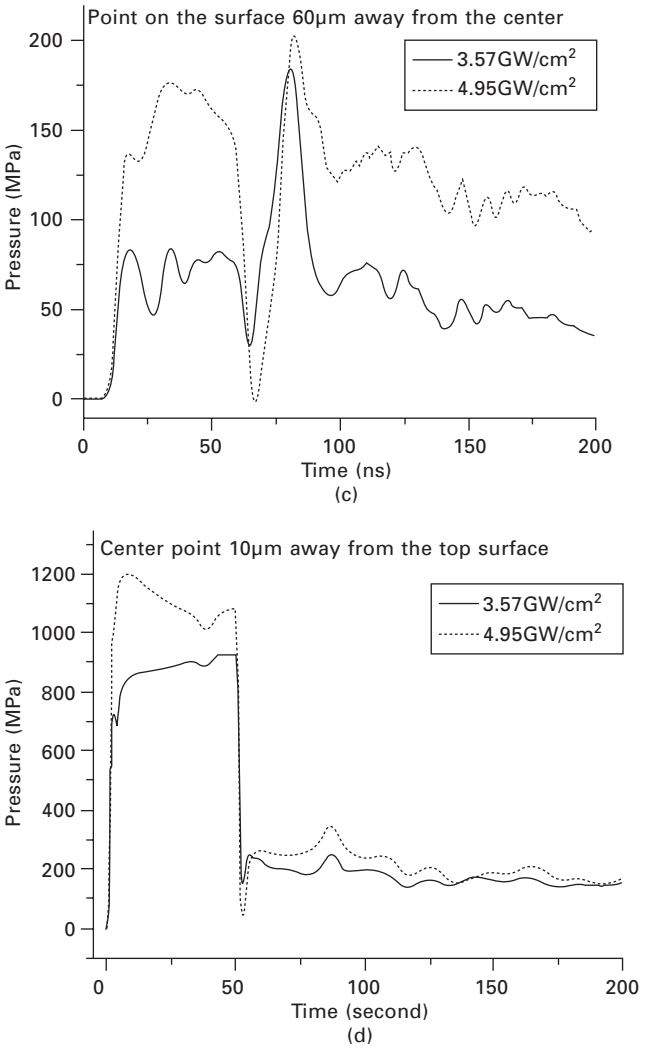

18.19 Continued

that the range and magnitude of compressive stress induced by 4.95GW/cm^2 are much larger than those by 3.57GW/cm^2. The range of compressive stress for 4.95GW/cm^2 is around ±200μm while that of 3.57GW/cm^2 is only ±100 μm. The effect of bending moment is relatively small compared with that of compressive stress since the bending angle is very small, about 0.1°. Therefore, the induced compressive stress plays a dominant role on the bending after loading. If the compressive stress distribution is wide, it is harder to generate downward bending. So it is more difficult to obtain convex shape for low energy than high energy in terms of compressive stress

distribution. Wave propagation of the point 60μm away from the center on the top surface as shown in Fig. 18.19(c) gives some insight into the difference of compressive stress distribution for these two cases. It can be seen that the pressure at that point for 4.95GW/cm^2 is two and a half times of that of 3.57GW/cm^2. However, shock wave propagation in depth direction is similar for both cases as shown in Fig. 18.19(d). The difference of wave propagation in the depth and surface directions may be due to the material volume that can be compressed. For either case, there is little material which can be compressed in depth direction because the thickness is too thin. But for the surface direction, there is enough material for compressing.

The tension caused by compressive stress in the 4.95GW/cm^2 case, which exerts bulging in the specimen, will restrain downward bending significantly compared to the 3.57GW/cm^2 case. That is why the downward bending of 4.95GW/cm^2 is smaller than that of 3.57GW/cm^2. After the combined effect of bending moment and compressive stress overcomes the downward effect caused by the inertia, the reverse bending follows. The reverse magnitude is mostly determined by the induced compressive stress and not the bending moment. Hence, the reverse magnitude of 4.95GW/cm^2 case is larger than that of the 3.57GW/cm^2 case. For the 4.95GW/cm^2 case, the compressive stress even overcomes the opposite bending moment and results in upward bending.

Influence of thickness on the forming process

The global deformation and residual stress pattern by μLPF are determined by various parameters, such as laser pulse energy, target material, and thickness of metal sheet, etc. Here, thickness effects are investigated.

Figure 18.20 gives the global deformation for the 200 μm copper sample by μLPF under the 4.95GW/cm^2 condition. It is clear that it is convex bending and the magnitude of the deformation is around 5 μm, corresponding to a bending angle of 0.057°. As seen in Fig. 18.21, as thickness increases, the induced compressive stress is almost the same as that of 100 μm, and consequently the global deformation decreases because the moment of inertia increases. In addition, the bending mode is the same as that of 100 μm under the same conditions. Also, the simulation results are comparable with the experimental results as shown in Fig. 18.20. According to the above results, we may say that thickness has almost no effect on residual stress distribution. The residual stress distribution by both simulation and experiment is shown in Fig. 18.21. Both show the same trend and are comparable, but the magnitude of the stress is a little smaller than that of 100 μm on both sides.

Laser peen forming of thick strips has been investigated by (Hackel and Harris, 2002), but there is no concave bending reported. Wang *et al*. (2007) showed that concave bending is possible if material thickness is in the micron

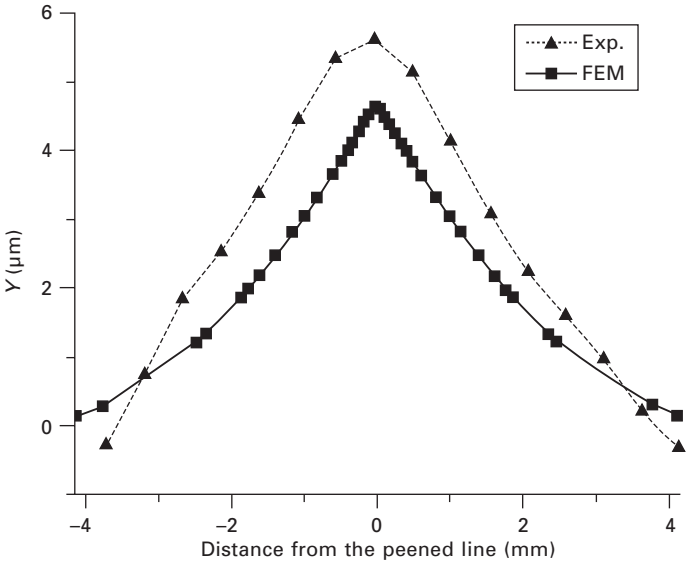

18.20 The curvature resulted from μLPF with the condition of 4.95GW/cm^2 laser intensity for 200μm copper sample.

range. Therefore, the downward bending effect caused by impacts (loading) and the followed inertia is very small in Hackel *et al*. (2000) since the inertia of moment, which is proportional to the cube of thickness, is big enough to prevent the downward bending. So the convex curving effect mainly results from surface elongation.

18.5.3 Effects of anisotropy

Further advancement in the micro-scale laser peen forming (μLPF) led to studies in single crystals. Experimental and numerical study has been performed by Wang *et al*. (2008b) who applied laser shocks on the aluminum single crystals with (001) crystallographic orientation of the surface. The train of laser shocks has been placed along the (110) crystallographic direction in order to achieve plane strain deformation, similar to the μLSP studies described in previous section. By doing this only three effective in-plane slip systems are activated (Rice, 1987) which simplifies the analysis. The residual stress characterization has been performed on top and bottom surfaces following the scheme on the polycrystalline copper specimens resulting in similar conclusions. Further, lattice rotation measurements were made via electron backscatter diffraction (EBSD). These measurements indeed confirmed that plane stain condition is achieved. Numerical analysis incorporated development of finite element model (FEM) based on single crystal plasticity. The problem

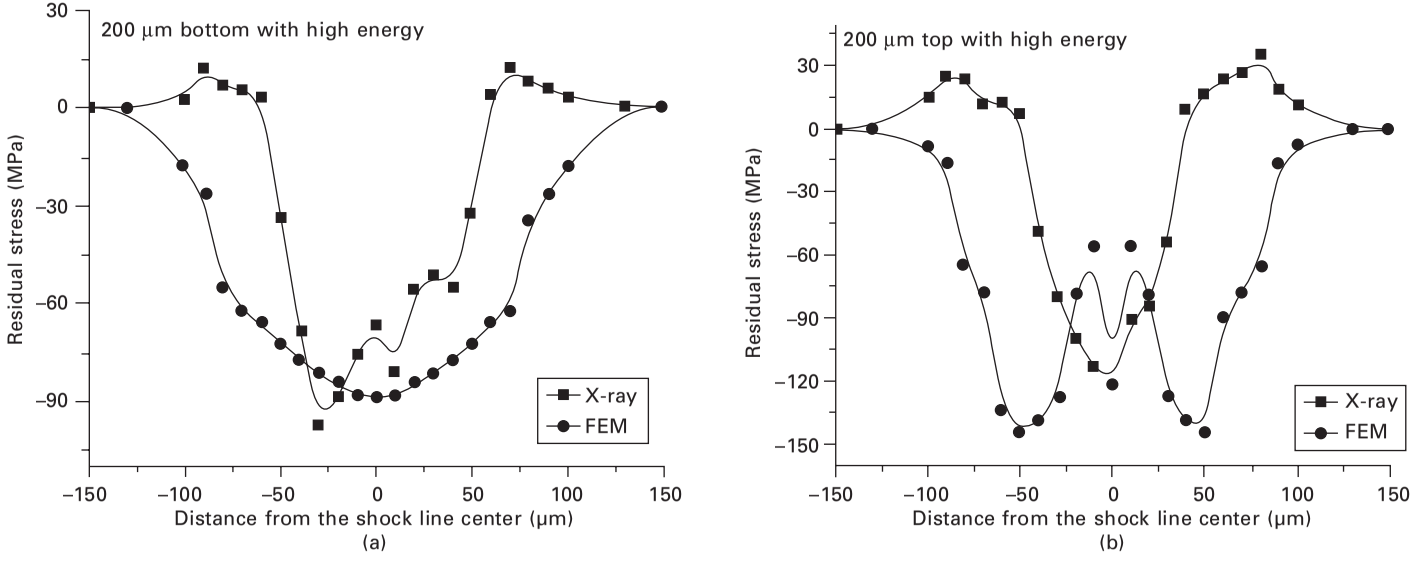

18.21 Residual stress distribution by X-ray micro-diffraction and FEM simulation: (a) 200 μm sample bottom with high energy; (b) 200 μm sample top with high energy.

is approximated as punch with non-uniform load (Rice, 1973; Wang *et al*., 2008a) to investigate local and global deformation under Gaussian pressure loading induced by laser shock. The model developed is two dimensional, plane strain and quasi-static and although gross simplification of actual process which is highly dynamic, it gives insight about the nature of deformation process. In addition, experimental findings of displacement and residual stress characterization agree well with numerical predictions (Wang *et al*., 2008b).

A total of three slip systems are active under plane strain condition *i*, *ii*, and *iii*. Because of zero Schmid's factor for slip system *ii*, its resulting shear strain is almost zero. Further due to symmetry of yield surface deformation caused by slip systems *i* and *iii* is anti-symmetric with respect to the vertical axis passing through the middle of the load. Plate XXIII (between pages 428 and 429) shows the shear strain distributions for the slip system *i* as well as the total shear strain by FEM simulation, that is, Plate XXIII(a) shows the shear strain distribution caused by slip system *i*, and Plate XXIII(b) is for the total shear strain. As seen in Plate XXIII, the shear strains resulting from μLPF have certain distributional patterns. It is of great interest to understand the logic behind these patterns.

In μLSP domain of interest is considered to be semi-infinite and deformation is local. On the other hand, in μLPF nature of deformation mechanism is different and global deformation has to be taken into account. Width of Gaussian pressure loading is an order of magnitude smaller than width of specimen, and effect of finite geometry has to be taken into account. In order to geometrically construct a slip line field, at first a similar approach as in μLSP has been taken. End points of the punch represent singular points (Wang *et al*., 2008a). However, from numerical simulation it appears that from the perspective of global deformation, Gaussian pressure loading in μLPF appears more as a point load. It further seems that loading can be seen as the point of singularity in which a centered fan is placed. A suggested slip line field geometrically constructed this way is depicted in Fig. 18.22. Shear strain in top half plane should appear only in the area enclosed by $Q_1Q_4Q_7O$. Plate XXIII(b) shows numerical results of the total shear strain with slip line field superimposed for the comparison purposes. From Plate XXIII(b) it can be seen that shear strain occurs only within the area inside of the sectors. Furthermore, slip system *i* is active in sectors, enclosed by $Q_1Q_2OQ_1$, OQ_2Q_3O, OQ_3Q_4O, and OQ_6Q_7O as shown in Fig. 18.22. Again, after superposition of slip sectors and numerical results (Plate XXIII(a)) we see that the numerical solution of shear strain distribution for slip system *i* agree fairly well with the proposed explanation.

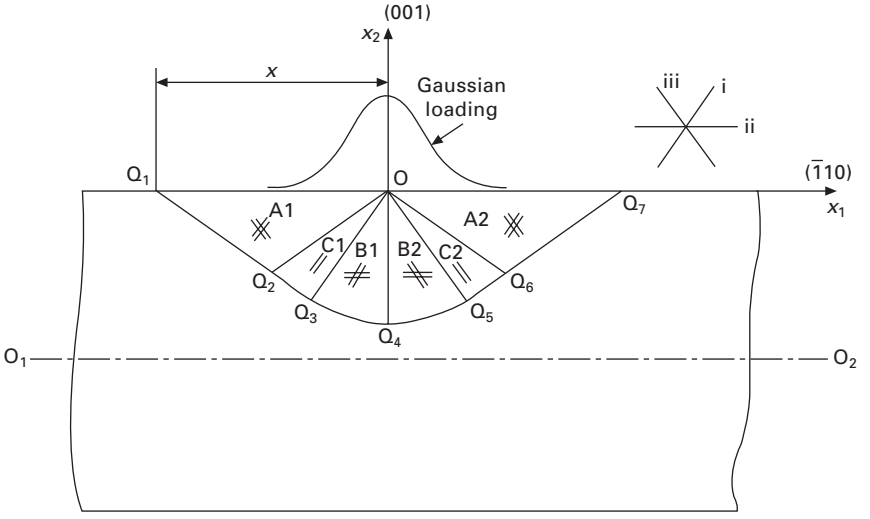

18.22 Geometry of slip line field for a Gaussian pressure distribution of load in micro-scale laser peen forming.

18.6 References

Asaro, R. J., 1983, "Micromechanics of Crystals and Polycrystals," *Advances in Applied Mechanics*, 23, pp. 1–115.

Asaro, R. J. and Needleman, A., 1985, "Texture Development and Strain Hardening in Rate Dependent Polycrystals," *Acta Metallurgica*, 33 (6) pp. 923–953.

Bao, J. and Yao, Y. L., 2001, "Analysis and Prediction of Edge Effects in Laser Bending", *Journal of Manufacturing Science and Engineering,* 123, pp. 53–61.

Birnbaum, A. J. and Yao, Y. L., 2006, "The Effects of Laser Forming on Superelastic NiTi Shape Memory Alloys", *Int. Conf. on Appl. of Gas and Electro-Opt., 0.25.* art no. p529.

Birnbaum, A. J., Cheng, P. and Yao, Y. L., 2007, "The Effects of Clamping on the Laser Forming Process," *Journal of Manufacturing Science and Engineering,* 129, pp. 1035–1044.

Booker, J. R. and Davis, E. H., 1972, "A General Treatment of Plastic Anisotropy Under Conditions of Plane Strain," *Journal of the Mechanics and Physics of Solids*, 20, pp. 239–250.

Cao, N. Krishnan, Z. Wang, H. Lu, W. K. Liu and A. Swanson, 2004, ASME *J. Manuf. Sci. Eng.* 126, 642.

Caruso, A., Guskov, S. Y., Doskach, I. Y., Zmitrenko, N. V., Rozanov, V. B. and Strangio, C., 2002, "Laser-Generated Weak Shock Wave Propagation Dynamics in the Solids," *Proc. SPIE*, 4424, pp. 508–511.

Chen, H., Yao, Y. L. and Kysar, J. W., 2004a, "Spatially Resolved Characterization of Residual Stress Induced by Micro Scale Laser Shock Peening," *ASME Transactions Journal of Manufacturing Science and Engineering*, 126, pp. 226–235.

Chen, H., Kysar, J. W. and Yao, Y. L., 2004b, "Characterization of Plastic Deformation Induced by Microscale Laser Shock Peening," *Journal of Applied Mechanics*, 71, 713.

Cheng, J. and Yao, Y. L., 2002, "Microstructure Integrated Modeling of Multiscan Laser Forming," *Journal of Manufacturing Science and Engineering,* 124, pp. 379–388.

Cheng, P. and Yao, Y. L., 2005, "The Influence of Sheet Metal Anisotropy on Laser Forming Process," *Journal of Manufacturing Science and Engineering*, 127, pp. 572–582.

Cheng, P., Yao, Y. L., Liu, C., Pratt, D. and Fan, Y., 2005, "Analysis and Prediction of Size Effect on Laser Forming of Sheet Metal" *SME J. of Manufacturing Processes*, 7(1), 2005, pp. 28–41.

Cheng, P., Fan, Y., Zhang, J., Mika, D., Graham, M., Zhang, W., Marte, J., Jones, M. and Yao, Y. L., 2006a, "Laser Forming of Varying Thickness Plate – Part I: Process Analysis," *Journal of Manufacturing Science and Engineering*, 128, pp. 634–641.

Cheng, P., Fan, Y., Zhang, J., Mika, D., Graham, M., Zhang, W., Marte, J., Jones, M. and Yao, Y. L., 2006b, "Laser Forming of Varying Thickness Plate – Part II: Process Synthesis," *ASME Trans. J. of Manufacturing Science and Engineering*, 128, pp. 642–650.

Clauer, A. H. and Holbrook, J. H., 1981, "Effects of Laser Induced Shock waves on Metals," *Shock Waves and High Strain Phenomena in Metals – Concepts and Applications*, New York, Plenum, pp. 675–702.

Clauer, A. H. and Lahrman, D. F., 2001, "Laser Shock Processing as a Surface Enhancement Process," *Key Engineering Materials*, 197, pp. 121–142.

Cottet, F. and Boustie, M., 1989, "Spallation Studies in Aluminum Targets Using Shock Waves Induced by Laser Irradiation at Various Pulse Durations," *J. Appl. Phys.*, 66(9), pp. 4067–4073.

Cullity, B. D., 1978, *Elements of X-ray Diffraction*, 2nd edn, Addison-Wesley Publishing Company, Inc. London.

Esser, G., Schemidt, M. and Dirscherl, M., 2003, *Proc. SPIE* 5063, 177.

Fan, Y., Yang, Z., Cheng, P, Egland, K. and Yao, Y. L., 2005, "Effects of Phase Transformations on Laser Forming of Ti-6Al-4V Alloy," *Journal of Applied Physics*, 98104904.

Fan, Y., Wang, Y., Vukelic, S. and Yao, Y. L., 2007, "Numerical Investigation of Opposing Dual Sided Microscale Laser Shock Peening," *J. of Manufacturing Science and Engineering*, 129, pp. 256–264.

Geiger, M., Kleiner, M., Eckstein, R., Tiesler, N. and Engel, U., 2001, *CIRP Ann.*, 50, 445.

Hackel, L. A. and Harris, F. B., 2002, US Patent No. 6410884.

Hammersley, G., Hackel, L. A. and Harris, F., 2000, "Surface Prestressing to Improve Fatigue Strength of Components by Laser Shot Peening," *Optics and Lasers in Engineering*, 34, 327–337.

Hill, R., 1950, *The Mathematical Theory of Plasticity*, Clarendon Press.

Kysar, J. W., Gan, Y. X. and Mendez-Arzuza, G., 2005, "Cylindrical Void in a Rigid-Ideally Plastic Single Crystal. Part I: Anisotropic Slip Line Theory Solution for Face-Centered Cubic Crystals," *International Journal of Plasticity*, 21, pp.1481–1520.

Li, W. and Yao, Y. L., 2001a, "Numerical and Experimental Investigation of Convex Laser Forming Process," *Journal of Manufacturing Processes,* 3, pp. 73–81.

Li, W. and Yao, Y. L., 2001b "Laser Forming with Constant Line Energy," *Int. J. Advanced Manufacturing Technology,* 17, pp. 196–203.

Liu, C., Yao, Y. L. and Srinivasan, V., 2004 "Optimal Process Planning for Laser Forming of Doubly Curved Shapes," *ASME Trans. J. of Manufacturing Science and Engineering*, 126, pp. 1–9.

Magee, J., Watkins, K. G., Steen, W. M., Calder, N., Sidhu, J. and Kirby, J., 1997, "Edge Effects in Laser Forming," *Proceedings of the LANE,* pp. 399–408.

Masubuchi, K., 1992, "Studies at MIT related to applications of laser technologies to metal fabrication," *Proceedings of LAMP'92*, pp. 939–946.

Merklen, M., Hennige, T. and Geiger, M., 2001, "Laser Forming of Aluminum and Aluminum Alloys-Microstructural Investigation," *Journal of Materials Processing Technology,* 115, pp.159–165.

Mok, C.-H., 1968, "Effects of Solid Strength on the Propagation and Attenuation of Spherical and Plane Shock Waves," *J. Appl. Phys.*, 39(4), pp. 2072–2081.

Namba, Y., 1986, "Laser Forming in Space," *Proc. International Conf. Lasers'85*, pp. 403–407.

Nemat-Nasser, S., Okinaka, T., Nesterenko, V. and Liu, M. Q., 1998, "Dynamic Void Collapse in Crystals: Computational Modelling and Experiments," *Philosophical Magazine A-Physics of Condensed Matter Structure Defects and Mechanical Properties*, 78(5), pp. 1151–1174.

Noyan, I. C. and Cohen, J. B., 1987, *Residual Stress : Measurement by Diffraction and Interpretation*, *Materials Research and Engineering*, Springer-Verlag, New York.

Ostendorf, A., Paschko, S., Von Busse, A., Bunte, J., Hustedt, M. and Fargas, M., 2004, "Laser Based Induction of the Two-way Memory Effect into Shape Memory Alloy Components", *Proc. of SPIE*, 5662, art. no. 95, pp. 586–592.

Otsu, M., Wada, T. and Osakada, K., 2001, *CIRP Ann.* 50, 141.

Peyre, P., Fabbro, R., Berthe, L. and Dubouchet, C., 1996, "Laser shock processing of materials, physical processes involved and examples of applications," *Journal of Laser Applications*, 8, pp. 135–141.

Peyre, P., Sollier, A., Chaieb, I., Berthe, L., Bartnicki, E., Braham, C. and Fabbro, R., 2003, "FEM simulation of residual stresses induced by laser Peening," *European Physical Journal: Applied Physics*, 23, pp. 83–88.

Pierce, D., Asaro, R. J. and Needleman, A., 1983, "Material Rate Dependence and Localized Deformation in Crystalline Solids," *Acta Metallurgica*, 31(12), pp. 1951–1976.

Rice, J. R., 1973, "Plane Strain Slip Line Theory for Anisotropic Rigid/Plastic Materials," *Journal of the Mechanics and Physics of Solids*, 21, pp. 63 –74.

Rice, J. R., 1987, "Tensile Crack Tip Fields in Elastic-Ideally Plastic Crystals," *Mechanics of Materials 6*, pp. 317–335.

Rose, J. L., Balasubramaniam, K. and Tverdokhlebov, A, 1989, "A Numerical Integration Green's Function Model for Ultrasonic Field Profiles in Mildly Anisotropic Media," *Journal of Nondestructive Evaluation*, 8(3), pp. 165–179.

Tverdokhlebov, A. and Rose, J., 1988, "On Green-Functions for Elastic-Waves in Anisotropic Media," *Journal of the Acoustical Society of America*, 83(1), pp. 118–121.

Ungar, T., Mughrabi, H., Ronnpagel, D. and Wilkens, M., 1984, "X-Ray Line-Broadening Study of the Dislocation Cell Structure in Deformed [001]-Orientated Copper Single-Crystals," *Acta Metallurgica*, 32(3), pp. 333–342.

Vollertsen, F., 1994, "An Analytical Model for Laser Bending," *Lasers in Engineering*, 2, pp. 261–276.

Vukelić, S., Wang, Y., Kysar, J. W. and Yao, Y. L., 2008a, "Comparative Study of Symmetric and Asymmetric Deformation of Al Single Crystal Under Micro Scale Shock Peening," *Journal of Mechanics of Materials and Structures*, 4, 89–105.

Vukelić, S., Wang, Y., Kysar, J. W. and Yao, Y. L., 2008b, "Dynamic Material Response of Aluminum Single Crystal under Micro Scale Laser Shock Peening," *Journal of Manufacturing Science and Engineering*, 131(3), 031015-1-013015-10.

Vukelic, S., Kysar, J. W. and Yao, Y. L., 2008c, "Grain boundary Response of Aluminum Bicrystal Under Micro Scale Laser Shock Peening," *International Journal of Solids and Structures*, 46, 3323–3335.

Wang, Y., Fan, Y., Vukelic, S. and Yao, Y. L., 2007, *J. Manuf. Process.*, 9, 1.

Wang, Y., Kysar, J. W. and Yao, Y. L., 2008a, "Analytical Solution of Anisotropic Plastic Deformation Induced by Micro-Scale Laser Shock Peening," *Mechanics of Materials*, 40 (3) pp. 100–114.

Wang, Y., Fan, Y., Kysar, J. W., Vukelic, S. and Yao, Y. L., 2008b, "Microscale laser peen forming of single crystal," *Journal of Applied Physics*, 103, 063525.

Zhang, W. and Yao, Y. L., 2000, "Microscale Laser Shock Processing – Modeling, Testing, and Microstructure Characterization," *J. Manuf. Process.*, 3(2), pp. 128–143.

Zhang, W. and Yao, Y. L., 2001, "Micro-scale Laser Shock Processing: Modeling, Testing, and Microstructure Characterization," *SME J. of Manufacturing Processes*, 3, pp. 128–143.

Zhang, W. and Yao, Y. L., 2002, "Microscale Laser Shock Processing of Metallic Components," *ASME Transactions Journal of Manufacturing Science and Engineering*, 124, (2), pp. 369–378.

Zhang, J., Cheng, P., Zhang, W., Graham, M., Jones, J., Jones, M. and Yao, Y. L., (2006), "Effect of Scanning Schemes on Laser Tube Bending," *Journal of Manufacturing Science and Engineering*, 128 pp. 20–33.

Zhou, M., Zhang, Y. and Cai, L., 2002, "Laser Shock Forming on Coated Metal Sheets Characterized by Ultrahigh-Strain-Rate Plastic Deformation," *Journal of Applied Physics*, 91, pp. 5501–5503.

Zhou, M., Zhang, Y. K. and Cai, L., 2003, "Ultrahigh-Strain-Rate Plastic Deformation of A stainless-Steel Sheet with Tin Coatings Driven by laser Stock waves," *Applied Physics A – Materials Science and Processing*, 77, (3-4) 549–554.